NeuroImage 298 (2024) 120775

Contents lists available at ScienceDirect

NeuroImage

journal homepage: www.elsevier.com/locate/ynimg

Evaluation of cervical spinal cord atrophy using a modified SIENA approach

Ludovico Luchetti [a,b], Ferran Prados [c,d,e], Rosa Cortese [a], Giordano Gentile [b], Massimilano Calabrese [f], Marzia Mortilla [g], Nicola De Stefano [a], Marco Battaglini [a,b,*], the Alzheimer's Disease Neuroimaging Initiative[1]

[a] Department of Medicine, Surgery and Neuroscience, University of Siena, Siena, Italy
[b] Siena Imaging S.r.l., Siena, Italy
[c] NMR Research Unit, Queen Square MS Centre, Department of Neuroinflammation, UCL Queen Square Institute of Neurology, Faculty of Brain Sciences, University College London, London, United Kingdom
[d] Center for Medical Imaging Computing, Medical Physics and Biomedical Engineering Department, University College London, London, United Kingdom
[e] e-Health Center, Universitat Oberta de Catalunya, Barcelona, Spain
[f] Department of Neuroscience, Biomedicine and Movements, The Multiple Sclerosis Center of the University Hospital of Verona, Verona, Italy
[g] Anna Meyer Children's University Hospital-IRCCS, Florence, Italy

ARTICLE INFO

Keywords:
Spinal cord
MRI
Longitudinal atrophy
SIENA
Multiple Sclerosis
pSCVC

ABSTRACT

Spinal cord (SC) atrophy obtained from structural magnetic resonance imaging has gained relevance as an indicator of neurodegeneration in various neurological disorders. The common method to assess SC atrophy is by comparing numerical differences of the cross-sectional spinal cord area (CSA) between time points. However, this indirect approach leads to considerable variability in the obtained results. Studies showed that this limitation can be overcome by using a registration-based technique.

The present study introduces the Structural Image Evaluation using Normalization of Atrophy on the Spinal Cord (SIENA-SC), which is an adapted version of the original SIENA method, designed to directly calculate the percentage of SC volume change over time from clinical brain MRI acquired with an extended field of view to cover the superior part of the cervical SC.

In this work, we compared SIENA-SC with the Generalized Boundary Shift Integral (GBSI) and the CSA change. On a scan-rescan dataset, SIENA-SC was shown to have the lowest measurement error than the other two methods. When comparing a group of 190 Healthy Controls with a group of 65 Multiple Sclerosis patients, SIENA-SC provided significantly higher yearly rates of atrophy in patients than in controls and a lower sample size when measured for treatment effect sizes of 50%, 30% and 10%.

Our findings indicate that SIENA-SC is a robust, reproducible, and sensitive approach for assessing longitudinal changes in spinal cord volume, providing neuroscientists with an accessible and automated tool able to reduce the need for manual intervention and minimize variability in measurements.

1. Introduction

Volumetric analysis of magnetic resonance images (MRI) of the spinal cord (SC) allows both the mapping of physiological evolution and the assessment of pathological deviations in atrophy rates due to disease progression (Antonescu et al., 2018; Bonacchi et al., 2020; Ciccarelli et al., 2019; Kearney et al., 2015; Lersy et al., 2021; Lorenzi et al., 2020; Mariano et al., 2021; Ziegler et al., 2018). However, measurements of SC atrophy are not as robust and reliable as brain atrophy measurements and, although new assessment methods have been suggested, there remains a significant disparity between brain and SC volumetric evaluations (Rovira and de Stefano, 2016). The challenges arise mainly from

* Corresponding author at: Department of Medicine, Surgery and Neuroscience, University of Siena, Siena, Italy.
E-mail address: battaglini@sienaimaging.it (M. Battaglini).

[1] Data used in preparation of this article were obtained from the Alzheimer's Disease Neuroimaging Initiative (ADNI) database (adni.loni.usc.edu). As such, the investigators within the ADNI contributed to the design and implementation of ADNI and/or provided data but did not participate in analysis or writing of this report. A complete listing of ADNI investigators can be found at: http://adni.loni.usc.edu/wp-content/uploads/how_to_apply/ADNI_Acknowledgement_List.pdf.

https://doi.org/10.1016/j.neuroimage.2024.120775
Received 22 December 2023; Received in revised form 12 July 2024; Accepted 2 August 2024
Available online 4 August 2024

the small size and mobility of the SC, causing MR signal inhomogeneity and impacting SC tissue segmentation (Rovira and de Stefano, 2016).

Currently, two approaches are employed to evaluate longitudinal volumetric changes over time. The first method involves comparing the cross-sectional area (CSA) or SC volume using segmentation maps independently obtained at each timepoint (Amann et al., 2016; De Leener et al., 2014; Losseff et al., 1996; Lukas et al., 2021; Stroman et al., 2014; Wheeler-Kingshott et al., 2014). This approach indirectly estimates atrophy rates but is limited by inaccuracies in segmentation maps due to partial volume effects. Additionally, this segmentation-based method often requires manual refinement of masks, introducing variability based on the operator's experience, workload, and fatigue. The second approach relies on SC-segmented masks that are registered on a common reference space (Prados et al., 2020; Valsasina et al., 2022). Previous studies have demonstrated that registration algorithms offer higher accuracy compared to segmentation methods, making this type of analysis more robust and reliable (Agosta et al., 2007; Cohen et al., 2012; Cohen-Adad et al., 2011; Moccia et al., 2019; Smith et al., 2007). In the case of SC, achieving precise visualization of the vertebrae is essential for accurately registering two SC MRI scans. Additionally, dedicated MRI analysis libraries have developed strategies for automatic cord segmentation (Gros et al., 2019; Prados et al., 2016; Yiannakas et al., 2016), tools for correcting intensity inhomogeneity (Tustison et al., 2010), and procedures for longitudinally evaluating volumetric differences through the study of co-registered image intensities (Prados et al., 2020; Smith et al., 2002; Valsasina et al., 2022).

Here we introduce SIENA-SC, an innovative and fully automated method designed for quantifying upper cervical spinal cord (SC) atrophy using a pair of sagittal and coronal brain MRI scans. SIENA-SC is built upon the foundational principles of SIENA (Smith et al., 2002), a tool within the FMRIB software library (FSL) (https://fsl.fmrib.ox.ac.uk/fsl/fslwiki), which is employed to evaluate edge displacement for each voxel at the interface of the spinal cord and cerebrospinal fluid in co-registered images. The approach involves the calculation of local shift of borders by assessing the distance of the zeros of the derivatives in 1-dimensional profiles related to each voxel of the border and these zeros are invariant for global multiplication factors. By employing this approach, SIENA-SC may mitigate the impact of MRI intensity inhomogeneity, independently of the intensity values, resulting in decreased variability in measurements and improved accuracy and reliability in assessments.

The study was structured into two main parts. Firstly, the methodology section provides a comprehensive elucidation of the SIENA-SC pipeline. The second part includes a comparative analysis of SIENA-SC with a registration-based method (i.e., the generalized boundary shift integral - GBSI - Prados et al., 2020), and a segmentation-based method (i.e., CSA as evaluated by Spinal Cord Toolbox, SCT -De Leener et al., 2017). This comparison is conducted with the aim of assessing differences in several critical aspects:i) examining robustness using scan-rescan MRI data of Healthy Controls (HCs); ii) assessing reliability by evaluating the degree of concordance among the methods on the HCs cohort; iii) evaluating sensitivity in detecting pathological differences of Multiple Sclerosis (MS) patients compared with HCs. The final part of the study explores the potential benefits of incorporating SIENA-SC into clinical research. Specifically, it explores how SIENA-SC may impact sample size requirements in comparison to currently available tools, offering valuable insights into its practical utility.

2. Methods

2.1. The SIENA-SC workflow

This work presents a new fully automatic pipeline for longitudinal SC atrophy computation that can be split into three parts: SC segmentation at each timepoint, SC image registration to a subject common space, and finally computation of the tissue differences on the edge of the SC canal using the SIENA technique. These three steps are common with previous registration-based methods (Prados et al., 2020; Valsasina et al., 2022), but they have been readapted and optimized for the SIENA-SC pipeline. The presented pipeline can compute longitudinal SC atrophy from T1-weighted brain MRI scans (See Fig. 1). The computation of the atrophy is performed on all the visible upper cervical cord which is covered both by the field-of-view (FOV) of the baseline scan as well as the FOV of the follow-up scan. The SC masks obtained from the SIENA-SC pipeline have been used as input also for the estimation of the atrophy using GBSI and the CSA change.

2.1.1. Step 1–spinal cord segmentation

The first crucial step to obtain a total automated pipeline is the identification of the SC. For the purpose of this study and to avoid any manual intervention we used the fully automatic deep learning algorithm provided by SCT library v.5.5 (sct_deepseg_sc) (Gros et al., 2019).

Before running sct_deepseg_sc, both MRI images were standardized to 1mm isotropic voxel size, and the FOV of the input images was limited to the spinal cord area.

To do this, the brainstem from the Harvard-Oxford subcortical structural atlases (HarvardOxford-sub-maxprob-thr50-1mm.nii.gz) available in FSL was chosen as the neurological reference for defining the bounding box to crop the FOV of the images.

The brainstem mask was resampled from the atlas in MNI152 space to the native T1-weighted images and eroded 5 times. The lower slice of the brainstem mask, approximately where the medulla oblongata joins the SC, was taken as a reference point to remove all the regions above the lower part of the brainstem. This step was performed to isolate the SC section and to improve the performance of the segmentation and subsequent registration step of the SC. Subsequently, sct_deepseg_sc was applied to the modified images.

The obtained SC masks were used as input to perform intensities correction in step 2.

2.1.2. Step 2–spinal cord image registration

In this second step, a series of image processing techniques, as described in the studies by Prados et al. (2020), Valsasina et al. (2022), are applied. These are used to minimize image noise, homogenize gray scales, straighten the SCs and align them in a half-way space. Prior to the registration on the half-way space, an additional step was introduced. This step involved re-segmenting the spinal cord to enhance accuracy and mitigate bias arising from intense intensity variations caused by MRI artifacts between scans. The segmentation was repeated on the input images, which had undergone denoising and inhomogeneity correction, using a propagation segmentation algorithm (De Leener et al., 2014). This algorithm used as input the centerline derived from the previously computed masks. Subsequently, the straightened images were aligned to the common halfway-space using an affine transformation through an inverse-consistent and symmetric algorithm (Modat et al., 2014), and masks corresponding to each time-point were resampled to the same space using nearest neighbor interpolation.

At this stage, two further refinements were made to the masks. Firstly, to address the potential loss of accuracy caused by resampling a mask into a different image space, we applied a smoothing technique to the mask borders. This smoothing was achieved using a diamond-connectivity of the voxels, ensuring a more precise and refined representation of the mask boundaries. Secondly, the resampled segmentation masks on the halfway space were merged and the upper and lower portions of the SC mask that were not captured by both scans were removed. This step ensured that the masks had consistent coverage length between the two timepoints. Such adjustments were necessary due to potential variations in the SC section caused by differences in the number of slices between timepoints (i.e. different orientation and/or positioning of the subject in the scanner).

Finally, the segmentation masks obtained at this point were used as input for the computation of the atrophy with the three methods: SIENA-

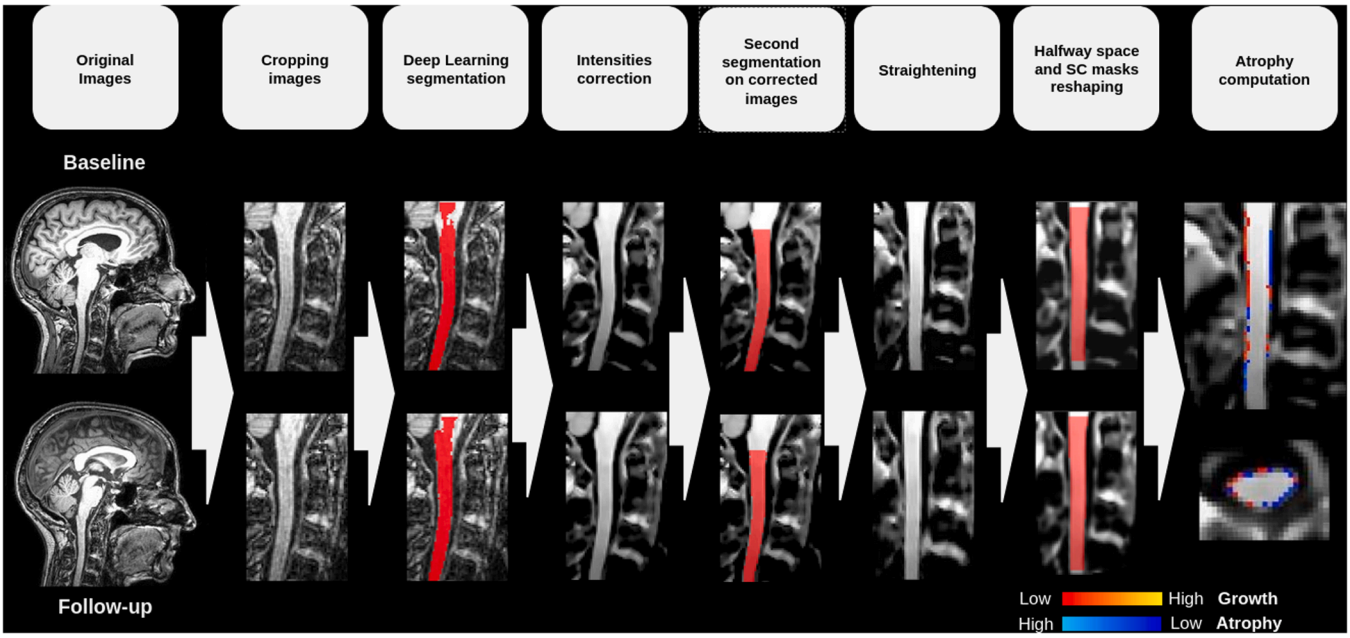

Fig. 1. SIENA-SC image processing pathway showing baseline (first line) and follow-up images (second line).

SC, GBSI and CSA change.

2.1.3. Step 3–atrophy computation using SIENA

As final step, the percentage Spinal Cord Volume Change (pSCVC) was estimated between the two aligned cord images using the SIENA algorithm principles. This involved estimating the mean perpendicular surface motion based on the masks' generated edge points, with the exclusion of flow in the z-direction (to have a 2D evaluation of atrophy along the SC). This was then converted into a pSCVC measurement.

To make the pSCVC estimation robust, the SIENA method internally corrects for possible small differences in image resolution and/or misalignment by calculating a calibration factor. Briefly, two pSCVCs are calculated between the original images and a couple of artificially generated images obtained by varying the voxel dimensions (one increasing and one decreasing from the same scale factor). These two pSCVC are then averaged. Given that the "nominal" pSCVC is known, once fixed the scale factor, a calibration factor can be obtained by dividing the "nominal" changes by the averaged pSCVC. Considering that the calculated pSCVC depends on the number of edge points and that this number is roughly 100 smaller for the SC than for the brain image (determined heuristically on a separated dataset not included in the analysis), we adjusted the scale factor accordingly by dividing for one hundred. Details of the analysis is shown in Supplementary Material, Section A.

To increase robustness, the "forward" and "backward" pSCVC were calculated for each pair of images swapping baseline and follow-up images. The average value of the "forward" and "backward" atrophy results was the final pSCVC.

2.2. MRI data

The gathered population has been categorized into three distinct sets of MRI data, each comprising different groups: a scan rescan dataset with 13 HC subjects, 190 HC subjects, and 65 MS subjects. The characteristics of the population are shown in Table 1.

All subjects had two brain 3D-T1 weighted images acquired in sagittal orientation using a 3T MRI scanner. Details of the MRI acquisition are in Table 2.

Notably, data related to the HC group utilized in this study were obtained from the Alzheimer's Disease Neuroimaging Initiative (ADNI) database (adni.loni.usc.edu). The ADNI was launched in 2003 as a public-private partnership, led by Principal Investigator Michael W. Weiner, MD. The primary goal of ADNI has been to test whether serial magnetic resonance imaging (MRI), positron emission tomography (PET), other biological markers, and clinical and neuropsychological assessment can be combined to measure the progression of mild cognitive impairment (MCI) and early Alzheimer's disease (AD). For up-to-date information, see www.adni-info.org.

Table 1
Population demographics. Center 1: Florence. Center 2: Verona. *Scan-rescan MRIs were performed within the same day.

	Scan rescan dataset	Healthy Control	Multiple Sclerosis
Number (Female)	13 (6)	190 (99)	Center 1: 10 (7) Center 2: 55 (45)
Age (years): Mean [Median] ± SD [min-max]	39 [39.13] ± 9.4 [24.9-56.45]	74 [73.7] ± 5.7 [57-94]	Center 1: 39.5 [38.5] ± 12.9 [19-61] Center 2: 38.9 [37] ± 11.3 [16-65]
Follow-up (years): Mean ± SD	0*	1.2 ± 0.2	Center 1: 1.2 ± 0.4 Center 2: 1.4 ± 0.7
EDSS	NA	NA	Center 1: 1.3 ± 0.3 Center 2: 1.7 ± 1.5
Disease Duration	NA	NA	Center 1: 8.9 ± 1.7 Center 2: 2.4 ± 4.6

2.2.1. Scan rescan dataset

Thirteen healthy subjects (mean age: 39 ± 9.4 years; female sex=46.15%) underwent a scan-rescan brain MRI acquisition using a 3 T Philips at the Meyer Hospital in Florence, Italy. Each subject had two MRI acquisitions on the same day with repositioning between the two scans. 3D T1-weighted brain images were acquired in sagittal orientation with a 1mm isotropic voxel. The purpose for using this dataset was to assess the scan-rescan repeatability, providing insights into the robustness of the automated software's measurements. In this context, the pSCVC values should approach zero as subjects should not show any atrophy within a very short time (about 1 h).

Table 2
Scanner acquisition details for ADNI datasets, Florence and Verona Sites.

Site	Field Strength	Manufacturer	Echo Time (ms)	Repetition Time (ms)	Flip Angle	Pixel Bandwidth	Slice Thickness (mm)	Spacing Between slices (mm)
ADNI	3T	Siemens	3	2300	9	238	1.2	1.2
ADNI	3T	Philips	3.2	6.8	9	241	1.2	1.2
Florence	3T	Philips	4	10	8	175	1	1
Verona	3T	Philips	4	8	8	191	1	1

2.2.2. Longitudinal dataset

HCs data: 190 subjects (mean age: 74 ± 5.7 years; female sex=52.1%) with an average follow-up of 1.2 ± 0.2 years.

MS data: 65 subjects acquired at two Italian sites: 10 subjects from the Meyer Hospital in Florence, Italy, (mean age: 40 ± 12.9 years; follow-up: 1.2 ± 0.4; female sex=70%) and 55 subjects from the University Hospital of Verona, Italy (mean age: 39 ± 11.3 years; follow-up: 1.4 ± 0.7; female sex=81.81%).

2.3. Ethics statement

Consent forms were approved by each relevant institutional review boards of Verona and Firenze and all patients gave written informed consent. The study was approved by the University of Siena ethics committee and received the reference number ECS00000017-THE.

2.4. Statistical Analysis

The present study compared the pSCVC measurements as assessed with SIENA-SC, GBSI and CSA methods.

The statistical analysis was performed using MATLAB Release R2020a. Significance level was set to $P < 0.05$. The results are shown in mean, standard deviation, and standard error. The yearly rate of atrophy was evaluated before performing statistics, except for the scan-rescan dataset.

Paired t-student was employed to compare pSCVC in the scan-rescan dataset (Battaglini et al., 2018; Nakamura et al., 2018).

Pearson's correlation has been used to evaluate the degree of concordance between the different measurements obtained by the different methods. The Bland Altman plot was used to test for the presence of systematic bias.

After testing with the MATLAB function lillietest the normal distribution of the residuals, a linear regression model has been used to measure the sensibility of the methods in discriminating HC subjects from MS patients. SIENA-SC, GBSI and CSA change were the dependent variables, and subject group (i.e., HC or MS), age, and sex were the covariates. Results are shown as the coefficient of pSCVC change in MS patients, 95% confidence interval, and p-values. Because of the exploratory nature of these analyses, we did not perform the correction for multiple comparisons.

To evaluate the precision of each method, we computed the sample size for a hypothetical trial with 80% power at the 5% significance level and looked for 50%, 30% and 10% treatment effects.

The pSCVC obtained from CSA measurements was determined by calculating the CSA difference between two consecutive time-points. The difference was then divided by the CSA of the first time-point and the result was multiplied by one hundred.

3. Results

3.1. Comparison between methods using healthy controls

3.1.1. Robustness: scan-rescan dataset

The pSCVC of SIENA-SC showed lower measurement error (mean: -0.06%; SD: ±0.18; SE: 0.03) compared to GBSI (mean: -0.12%; SD: ± 0.73; SE: 0.13; p<0.005) and CSA change (mean: 0.58%; SD: ± 2.2; SE: 0.32; p<10E-10). GBSI pSCVC showed lower measurement error compared with CSA (p<0.01). See Fig. 2.

3.1.2. Reliability: longitudinal dataset

On the HCs dataset, the annualized pSCVC showed no or minimal changes using all three methods (SIENA-SC: -0.05% ± 0.45; GBSI: -0.08% ± 1.6; CSA: 0.005% ± 3.1). Statistical comparisons did not show any difference in the measurements obtained with the three methods (SIENA-SC vs GBSI: p=0.85; SIENA-SC vs CSA change: p=0.78; GBSI vs CSA change: p=0.73). Example of quality of the images and atrophy rendering using the three methods are provided in Fig. 3.

3.1.3. SIENA-SC vs GBSI

Correlation of pSCVC between measurements obtained with SIENA-SC and GBSI was r=0.48, (p<0.05), mean absolute difference= -0.02%. The least-squares fit between SIENA-SC and GBSI is estimated at y=1.42x (R^2=0.16) (Smith et al., 2007). See Fig. 4 for a SIENA-SC vs GBSI Bland Altman. The strong asymmetry is driven by the differences in standard deviation between the two methods.

3.1.4. SIENA-SC vs CSA change

Correlation of pSCVC between SIENA-SC and CSA change measurements was r=0.29 (p<0.05), mean absolute difference=0.06%. The least-squares fit between SIENA-SC and CSA change is estimated at y=2.02x + 0.12 (R^2=0.09) (Smith et al., 2007). See Fig. 4 for a SIENA-SC vs. CSA Bland Altman. The strong asymmetry is driven by the differences in standard deviation between the two methods.

3.1.5. GBSI vs CSA change

Correlation of pSCVC between GBSI and CSA change was r=0.33 (p<0.05), mean absolute difference= 0.09%. The least-squares fit between GBSI and CSA change is estimated at y=0.63x-0.06 (R^2=0.11) (Smith et al., 2007). See Fig. 4 for a GBSI vs. CSA change Bland Altman.

3.2. Comparison between HC and MS

3.2.1. Linear regression model

The linear regression model adjusted by group (HC and MS), age and sex, showed a different rate of atrophy in MS patients compared to the HC using the three methods: SIENA-SC (Coeff: -0.54, 95%CI=[-0.87, -0.21], p<0.001); GBSI (Coeff: -0.84; 95%CI=[-1.81, 0.12], p=0.08); CSA change (Coeff: -1.92; 95%CI=[-3.82, -0.016], p=0.048). Raw values of the results are illustrated in Table 3 and Fig. 5.

3.2.2. Sensitivity: sample size

Considering the sample size estimation per arm for a clinical trial where SC atrophy could be an outcome to measure the response to treatment, SIENA-SC showed the lowest number of MS patients needed to observe a treatment effect (Table 4).

4. Discussion

Our study demonstrates the potentials of SIENA-SC, a fully automated, easy-to-use tool for calculating pSCVC using brain MRI acquisitions. This innovative approach extends the capabilities of the original SIENA method, designed for assessing brain structures, to quantify

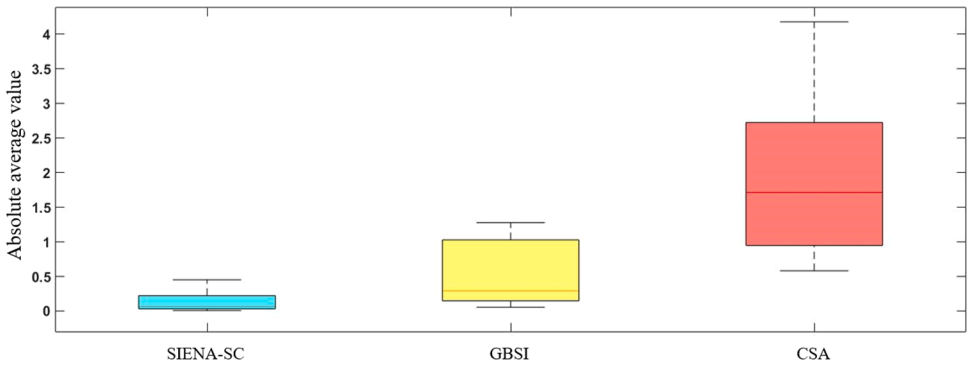

Fig. 2. Boxplot showing the comparison of the measurements using SIENA-SC, GBSI and CSA change on 13 HC subjects. The line inside the boxes indicates the median value. Results are shown in absolute values.

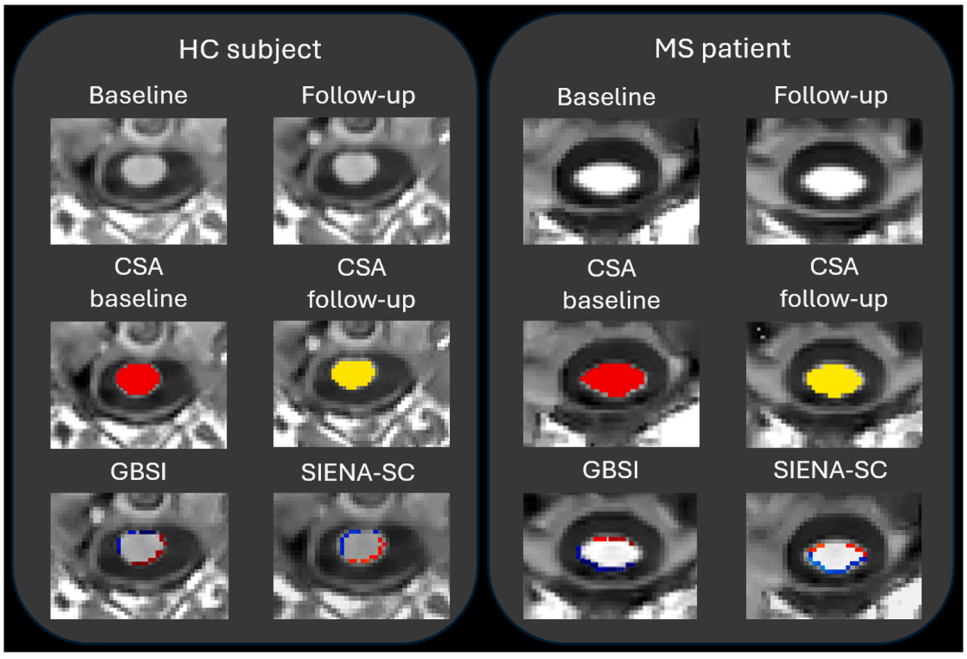

Fig. 3. Example of Spinal Cord atrophy assessment across the three methods on a HC (left) and MS (right) subject.

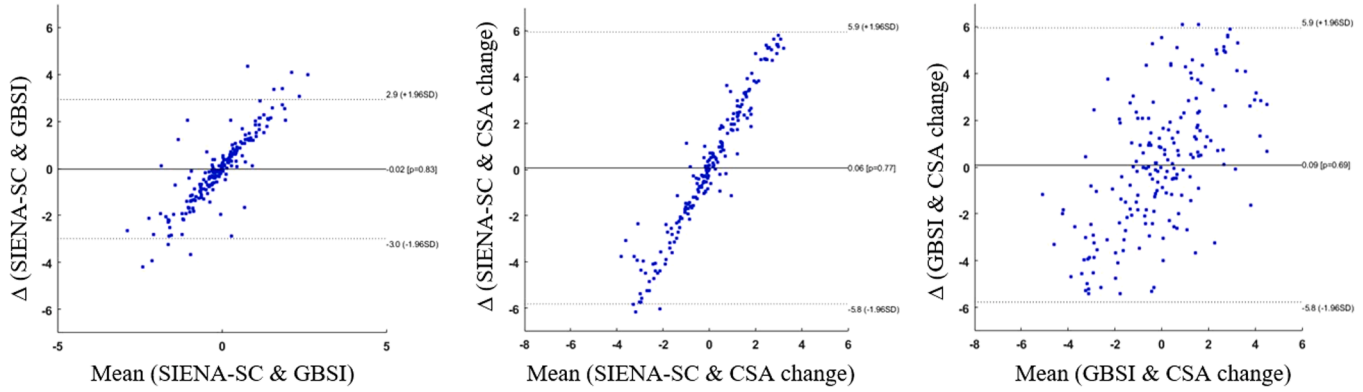

Fig. 4. Bland Altman plot showing the difference between SIENA-SC and GBSI (on the left); SIENA-SC and CSA change (in the middle); GBSI and CSA change (on the left).

upper cervical SC atrophy. By enabling the evaluation of SC atrophy from brain scans, our method has the ability to considerably reduce MRI scan times and associated costs, ultimately easing the burden on patients. Additionally, SIENA-SC offers the advantage of calculating pSCVC without requiring extensive computer engineering expertise and reducing inter-operator variability. To achieve this, we developed and tested a novel and optimized pre-processing procedure, which integrates and improves upon existing routines. As a result, SIENA-SC may

Table 3
Table showing the raw mean values, standard deviation, and standard error of pSCVC obtained with the three methods. SE: Standard Error.

	HC	MS	p-value
Annualized SIENA-SC [SE]	-0.05 ± 0.45 [0.03]	-0.6 ± 0.77 [0.09]	<0.001
Annualized GBSI [SE]	-0.08 ± 1.6 [0.12]	-1.14 ± 1.56 [0.19]	0.08
Annualized CSA change [SE]	0.005 ± 3.1 [0.22]	-1.52 ± 3.44 [0.42]	0.048

represent a valuable tool for both researchers and clinicians, streamlining the evaluation of SC atrophy and ensuring efficiency and reliability in the process.

SIENA-SC starts with a pre-processing step based on an artificial intelligence freely available tool (Gros et al., 2019). This initial stage eliminates the need for operator intervention necessary for the identification of the initial mask of the spine. Notably, this approach can stand on its own, making both GBSI and CSA fully automated. Indeed, the same generated cord masks have been used for the atrophy assessment in all three methods. To replicate the SIENA methodology for the analysis of SC atrophy, we optimized a registration procedure between two longitudinally acquired images using the niftyreg software package (https://github.com/KCL-BMEIS/niftyreg). For each timepoint, this procedure was implemented jointly using images and masks encompassing the dilated cord up to the vertebra. This provided the registration tool with a stationary reference, enhancing its accuracy. Further, the "straighten" step, which reduces the morphological and geometrical complexity of SC of both time points, improves the mutual registration of images when the halfway space is created.

Finally, SIENA-SC calculates the percentage change in atrophy by indirectly approximating local edge displacement. This is achieved by comparing the derivatives of intensities between the two images and applying a calibration factor that depends on the SC's size. The calibration factor serves to mitigate variability stemming from inherent differences between the two images. The optimization of this calibration factor was the final step implemented in our pipeline (See Supplementary Material, Section A).

In the present study, SIENA-SC demonstrated superior reliability in scan-rescan assessments of pSCVC compared to the other two methods, while no differences were observed when comparing SIENA-SC with the other two methods in the longitudinal dataset of HC. This is not surprising, due to the small biological variation of spinal cord volume in HC subjects (Moccia et al., 2019; Prados et al., 2020). Nevertheless, SIENA-SC demonstrated a smaller data dispersion, as indicated by the lower standard error. Furthermore, SIENA-SC showed significantly increased sensitivity in distinguishing between physiological and pathological conditions, along with the ability to reduce the necessary sample size for evaluating treatment effects in a cohort of MS subjects. Overall, these findings emphasize SIENA-SC's robustness, sensitivity, precision, and accuracy, establishing it as a valuable tool for assessing SC volume changes in neurological diseases.

The superior robustness of SIENA-SC and GBSI compared to CSA in the scan-rescan dataset can be attributed to the advanced capability of registration-based methods to account for partial volume effects, as demonstrated by previous studies (Prados et al., 2015; Smith et al., 2007). Such effects can introduce segmentation errors and increase variability when calculating cross-sectional areas. Traditional segmentation-based methods rely on numerical differences between areas obtained from hard segmentation at each time-point, often resulting in indirect estimates of atrophy and greater variability. This issue becomes more significant when dealing with scans featuring different intensity scales, varying voxel sizes, or other confounding factors such as subject repositioning, SC curvature, or noise. The similarities in approach between SIENA-SC and GBSI explain the moderate correlation (R=0.48) observed between these two methods in HC subjects. Conversely, this correlation becomes weaker when compared to CSA (SIENA-SC: R=0.29, GBSI: R=0.33). Thus, our analysis supports the well-established understanding of the greater reliability of registration-based methods compared with the segmentation-based ones (Moccia et al., 2019). For completeness, we repeated the correlation analysis also in MS patients obtaining similar results to the ones obtained in HC subjects (See Supplementary Material, Section B).

The superior performance exhibited by SIENA-SC in comparison to GBSI, despite sharing some pre-processing steps, may be attributed to the different approaches used to derive changes in atrophy from local intensities variations. SIENA-SC mitigates the impact of local random fluctuations in voxel intensities by comparing the profiles of the intensity derivatives, rather than directly assessing differences in voxel intensities. In contrast, GBSI reduces the global differences in two SC

Table 4
Estimated sample size per arm with all the three methods (Power=80%, 5% Significance level).

Software	Treatment Effect size %	Sample Size [CI] (MS Subjects)
SIENA-SC	50	54 [39 to 95]
	30	146 [107 to 217]
	10	1290 [933 to 1986]
GBSI	50	62 [36 to 135]
	30	167 [86 to 478]
	10	1483 [714 to 4287]
CSA	50	171 [59 to 5628]
	30	472 [157 to 2700]
	10	4224 [1859 to 8991]

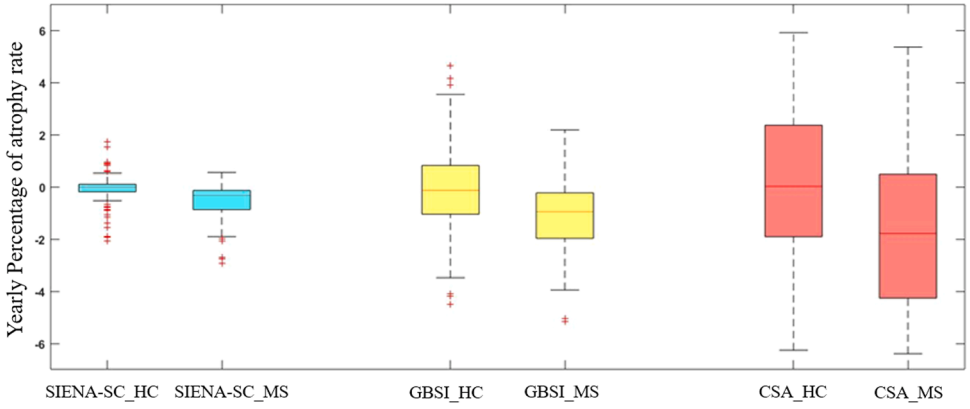

Fig. 5. Boxplot illustrates the comparison of the annualized percentage cord area changes obtained using SIENA-SC, GBSI and CSA change between healthy control and Multiple Sclerosis subjects.

images through prior intensity normalization and then directly compares voxel intensities. This approach could potentially be influenced by local fluctuations in voxel intensities, which are not fully recovered even after global intensity normalization. This suggests that SIENA-SC may be less biased by sources of variability in MRI signal, making it a very robust and reliable method for assessing SC atrophy.

The enhanced sensitivity was evaluated using a dataset of MS patients. Cervical SC atrophy has been a well-known feature in MS since the early stages and monitoring it holds clinical significance due to its correlation with increased disability (Lukas et al., 2015; Moccia et al., 2020; Valsasina et al., 2018). We demonstrated here a superior performance of SIENA-SC in differentiating between HCs and MS ($p<0.001$), in comparison to CSA ($p=0.048$) and GBSI ($p=0.08$). It is worth noting that this discrepancy might be in part related to the relatively small sample size dataset on which these tools were tested. Given the disparity in the number of MS patients between Center 1 and Center 2 (10 Vs 55), we did not incorporate center correction in the linear regression model, because of the strong overlapping between center 2 and the group of MS. As a confidence analysis, we performed a linear regression model adjusted for center, age, and sex within the MS group, revealing no significant differences between centers ($p=0.19$).

One of the main issues in using cervical SC atrophy as an outcome measure in clinical trial and observational studies is the large sample size required when using the CSA change (Moccia et al., 2017; Prados and Barkhof, 2018; Tur et al., 2018). Both SIENA-SC and GBSI demonstrated a notable advantage by yielding smaller sample size estimates when assessing treatment effects of 50-30-10% compared to CSA. SIENA-SC showed also a marginal reduction in sample size compared to GBSI, probably driven by the smaller error of the method, indirectly reducing the variance of yearly SC atrophy rates. Overall, the sample size estimates for SC atrophy measurements with SIENA-SC align in magnitude with those for brain atrophy obtained using registration-based methods (Storelli et al., 2023). Thus, these findings highlight the feasibility of using cervical SC atrophy as evaluated by SIENA-SC, as a suitable and promising endpoint for both clinical trials and observational studies. However, this study is just a proof of concept of the use of SIENA-SC and it is not without limitations. The first one concerns the retrospective design of the experiments involving MS patients. This led to two different issues: the MRI of MS patients did not have sequences in which SC lesions could be delineated, so it was not possible to obtain some useful information related to the impact of SC lesions in the evaluation of atrophy, and the HC and MS groups were strongly unbalanced by age. Despite these limitations, the absence of atrophy in HCs assessed by all methods and the significantly higher atrophy found in MS patients reassures for the consistency of SIENA-SC results. The second concerns the limited sample size of the groups analyzed, and for this reason SIENA-SC should be tested on larger datasets, both synthetic (Bautin and Cohen-Adad, 2021) and real, to test the default options in larger samples and to check the generalizability of the method. Further works should thoroughly investigate the use of SIENA-SC in assessing pathological deviations of atrophy in patients in specifically designed experiments. Furthermore, future improvements might entail tailoring SIENA-SC for dedicated spine MRI scans and integrating a feature to extract atrophy values from individual cervical sections.

In conclusion, this study introduces SIENA-SC, a novel method for the assessment of cervical cord atrophy. The software is fully automated, easy to use, and works with routinely acquired brain MRI sequences. The enhanced features of SIENA-SC could enable its utilization in evaluating physiological changes in extensive datasets (Battaglini et al., 2019), and explore its potential clinical applications for early disease detection and monitoring. Finally, the implementation of SIENA-SC can enhance the existing MRI biomarker portfolio by incorporating the measurement of cervical spinal cord atrophy, thus providing valuable insights into the evaluation of neurological diseases and enriching our understanding of these conditions (Cortese and Ciccarelli, 2018; Giovannoni et al., 2017; Uher et al., 2017).

Data and code availability statements

Data

Healthy Control data used in preparation of this article were obtained from the Alzheimer's Disease Neuroimaging Initiative (ADNI) database (adni.loni.usc.edu). As such, the investigators within the ADNI contributed to the design and implementation of ADNI and/or provided data but did not participate in analysis or writing of this report. A complete listing of ADNI investigators can be found at: http://adni.loni.usc.edu/wp-content/uploads/how_to_apply/ADNI_Acknowledgement_List.pdf

The rest of the data came from Meyer Hospital of Florence and the University Hospital of Verona and can be obtained upon submitting reasonable requests to the source institutions.

Code

SIENA-SC uses a miscellanea of software inside its pipeline.

- SCT has been used for spinal cord segmentation (sct_deepseg_sc and sct_propseg), straightening (sct_straighten_spinalcord) and can be found at https://spinalcordtoolbox.com/;
- N4BiasFieldCorrection is used for the inhomogeneity correction, and it is freely available as part of ANTs package at https://stnava.github.io/ANTs/. The following parameters have been used: full width at half maximum (FWHM) = 0.05, convergence threshold = 0.0001 and a maximum number of iterations = 1000;
- Denoising (niftkDenoise) is freely available as part of NifTK package at https://github.com/NifTK/NifTK;
- Registration between images has been performed using NiftyReg software package (reg_aladin) at https://github.com/KCL-BMEIS/niftyreg. The following parameter have been used: -pv 60 -pi 60 -maxit 15 -ln 8 -lp 8;
- fslroi has been used to crop the original T1 image with these parameters: fslroi T1.nii.gz OUTPUT_CROPPED.nii.gz xmin xlength ymin ylength zmin zlength 0 1. Siena_cal algorithm has been used to evaluate the calibration factor and Siena_diff algorithm has been used for the final atrophy computation. All the three the algorithms are part of the FSL package at https://fsl.fmrib.ox.ac.uk/fsl/fslwiki/ and they have been implemented in this paper using the above software packages, however, other software packages performing the same action could be used in each step of our pipeline.

CRediT authorship contribution statement

Ludovico Luchetti: Writing – review & editing, Writing – original draft, Visualization, Software, Methodology, Investigation, Formal analysis, Data curation, Conceptualization. **Ferran Prados:** Writing – review & editing, Writing – original draft, Supervision, Software, Methodology, Conceptualization. **Rosa Cortese:** Writing – review & editing, Writing – original draft, Supervision. **Giordano Gentile:** Writing – review & editing. **Massimilano Calabrese:** Resources. **Marzia Mortilla:** Resources. **Nicola De Stefano:** Writing – review & editing. **Marco Battaglini:** Writing – review & editing, Writing – original draft, Supervision, Methodology, Conceptualization.

Declaration of competing interest

The authors declare the following financial interests/personal relationships which may be considered as potential competing interests:

Nicola De Stefano reports financial support was provided by National Recovery and Resilience Plan (PNRR), and also relationship with Biogen, Merck, Novartis, Sanofi, Roche, Teva, FISM that includes:

consulting or advisory, funding grants, speaking and lecture fees, and travel reimbursement. Rosa Cortese reports a relationship with Roche, Merck Serono, Janssen, Novartis, Sanofi that includes: speaking and lecture fees and travel reimbursement. Ferran Prados reports a relationship with National Institute for Health and Care Research (NIHR) Biomedical Research Centres (BRC) at University College London (UCL) that includes: employment, funding grants, speaking and lecture fees, and travel reimbursement. Massimiliano Calabrese reports a relationship with Roche, Sanofi Genzyme, Merck Serono, Biogen Idec, Teva, and Novartis Pharma that includes: consulting or advisory, funding grants, speaking and lecture fees, and travel reimbursement. If there are other authors, they declare that they have no known competing financial interests or personal relationships that could have appeared to influence the work reported in this paper. If there are other authors, they declare that they have no known competing financial interests or personal relationships that could have appeared to influence the work reported in this paper.

Data availability

I have shared the information related to the data in the "data and code availability statements attachments"

Acknowledgments

Data collection and sharing for this project was funded by the Alzheimer's Disease Neuroimaging Initiative (ADNI) (National Institutes of Health Grant U01 AG024904) and DOD ADNI (Department of Defense award number W81XWH-12-2-0012). ADNI is funded by the National Institute on Aging, the National Institute of Biomedical Imaging and Bioengineering, and through generous contributions from the following: AbbVie, Alzheimer's Association; Alzheimer's Drug Discovery Foundation; Araclon Biotech; BioClinica, Inc.; Biogen; Bristol-Myers Squibb Company; CereSpir, Inc.; Cogstate; Eisai Inc.; Elan Pharmaceuticals, Inc.; Eli Lilly and Company; EuroImmun; F. Hoffmann-La Roche Ltd and its affiliated company Genentech, Inc.; Fujirebio; GE Healthcare; IXICO Ltd.; Janssen Alzheimer Immunotherapy Research & Development, LLC.; Johnson & Johnson Pharmaceutical Research & Development LLC.; Lumosity; Lundbeck; Merck & Co., Inc.; Meso Scale Diagnostics, LLC.; NeuroRx Research; Neurotrack Technologies; Novartis Pharmaceuticals Corporation; Pfizer Inc.; Piramal Imaging; Servier; Takeda Pharmaceutical Company; and Transition Therapeutics. The Canadian Institutes of Health Research is providing funds to support ADNI clinical sites in Canada. Private sector contributions are facilitated by the Foundation for the National Institutes of Health (www.fnih.org). The grantee organization is the Northern California Institute for Research and Education, and the study is coordinated by the Alzheimer's Therapeutic Research Institute at the University of Southern California. ADNI data are disseminated by the Laboratory for Neuro Imaging at the University of Southern California.

I would like to thank Damiano Marastoni e Agnese Tamanti for sharing data from Verona center.

Financial support project ECS00000017 Tuscany-Health Ecosystem—CUP B63C2200068007 spoke 6 Mission 4 Component 2 (M4C2)—investment 1.5 of the National Recovery and Resilience Plan (PNRR) funded by the European Union "Next Generation EU".

Supplementary materials

Supplementary material associated with this article can be found, in the online version, at doi:10.1016/j.neuroimage.2024.120775.

References

Agosta, F., Absinta, M., Sormani, M.P., Ghezzi, A., Bertolotto, A., Montanari, E., Comi, G., Filippi, M., 2007. *In vivo* assessment of cervical cord damage in MS patients: a longitudinal diffusion tensor MRI study. Brain 130, 2211–2219. https://doi.org/10.1093/brain/awm110.

Amann, M., Pezold, S., Naegelin, Y., Fundana, K., Andělová, M., Weier, K., Stippich, C., Kappos, L., Radue, E.W., Cattin, P., Sprenger, T., 2016. Reliable volumetry of the cervical spinal cord in MS patient follow-up data with cord image analyzer (Cordial). J. Neurol. 263, 1364–1374. https://doi.org/10.1007/s00415-016-8133-0.

Antonescu, F., Adam, M., Popa, C., Tuţă, S., 2018. A review of cervical spine MRI in ALS patients. J. Med. Life 11, 123–127.

Battaglini, M., Gentile, G., Luchetti, L., Giorgio, A., Vrenken, H., Barkhof, F., Cover, K.S., Bakshi, R., Chu, R., Sormani, M.P., Enzinger, C., Ropele, S., Ciccarelli, O., Wheeler-Kingshott, C., Yiannakas, M., Filippi, M., Rocca, M.A., Preziosa, P., Gallo, A., Bisecco, A., Palace, J., Kong, Y., Horakova, D., Vaneckova, M., Gasperini, C., Ruggieri, S., De Stefano, N., 2019. Lifespan normative data on rates of brain volume changes. Neurobiol. Aging 81, 30–37. https://doi.org/10.1016/j.neurobiolaging.2019.05.010.

Battaglini, M., Jenkinson, M., De Stefano, N., 2018. SIENA-XL for improving the assessment of gray and white matter volume changes on brain MRI. Hum. Brain Mapp. 39, 1063–1077. https://doi.org/10.1002/hbm.23828.

Bautin, P., Cohen-Adad, J., 2021. Minimum detectable spinal cord atrophy with automatic segmentation: investigations using an open-access dataset of healthy participants. Neuroimage Clin. 32, 102849 https://doi.org/10.1016/j.nicl.2021.102849.

Bonacchi, R., Pagani, E., Meani, A., Cacciaguerra, L., Preziosa, P., De Meo, E., Filippi, M., Rocca, M.A., 2020. Clinical relevance of multiparametric MRI assessment of cervical cord damage in multiple sclerosis. Radiology 296, 605–615. https://doi.org/10.1148/radiol.2020200430.

Ciccarelli, O., Cohen, J.A., Reingold, S.C., Weinshenker, B.G., Amato, M.P., Banwell, B., Barkhof, F., Bebo, B., Becher, B., Bethoux, F., Brandt, A., Brownlee, W., Calabresi, P., Chatway, J., Chien, C., Chitnis, T., Ciccarelli, O., Cohen, J., Comi, G., Correale, J., De Sèze, J., De Stefano, N., Fazekas, F., Flanagan, E., Freedman, M., Fujihara, K., Galetta, S., Goldman, M., Greenberg, B., Hartung, H.P., Hemmer, B., Henning, A., Izbudak, I., Kappos, L., Lassmann, H., Laule, C., Levy, M., Lublin, F., Lucchinetti, C., Lukas, C., Marrie, R.A., Miller, A., Miller, D., Montalban, X., Mowry, E., Ourselin, S., Paul, F., Pelletier, D., Ranjeva, J.P., Reich, D., Reingold, S., Rocca, M.A., Rovira, A., Schlaerger, R., Soelberg Sorensen, P., Sormani, M., Stuve, O., Thompson, A., Tintoré, M., Traboulsee, A., Trapp, B., Trojano, M., Uitdehaag, B., Vukusic, S., Waubant, E., Weinshenker, B., Wheeler-Kingshott, C.G., Xu, J., 2019. Spinal cord involvement in multiple sclerosis and neuromyelitis optica spectrum disorders. Lancet Neurol. 18, 185–197. https://doi.org/10.1016/S1474-4422(18)30460-5.

Cohen, A.B., Neema, M., Arora, A., Dell'Oglio, E., Benedict, R.H.B., Tauhid, S., Goldberg-Zimring, D., Chavarro-Nieto, C., Ceccarelli, A., Klein, J.P., Stankiewicz, J.M., Houtchens, M.K., Buckle, G.J., Alsop, D.C., Guttmann, C.R.G., Bakshi, R., 2012. The relationships among MRI-defined spinal cord involvement, brain involvement, and disability in multiple sclerosis. J. Neuroimaging 22, 122–128. https://doi.org/10.1111/j.1552-6569.2011.00589.x.

Cohen-Adad, J., El Mendili, M.M., Lehéricy, S., Pradat, P.F., Blancho, S., Rossignol, S., Benali, H., 2011. Demyelination and degeneration in the injured human spinal cord detected with diffusion and magnetization transfer MRI. Neuroimage 55, 1024–1033. https://doi.org/10.1016/j.neuroimage.2010.11.089.

Cortese, R., Ciccarelli, O., 2018. Clinical monitoring of multiple sclerosis should routinely include spinal cord imaging – Yes. Mult. Scler. J. 24, 1536–1537. https://doi.org/10.1177/1352458518778010.

De Leener, B., Kadoury, S., Cohen-Adad, J., 2014. Robust, accurate and fast automatic segmentation of the spinal cord. Neuroimage 98, 528–536. https://doi.org/10.1016/j.neuroimage.2014.04.051.

De Leener, B., Lévy, S., Dupont, S.M., Fonov, V.S., Stikov, N., Louis Collins, D., Callot, V., Cohen-Adad, J., 2017. SCT: spinal cord toolbox, an open-source software for processing spinal cord MRI data. Neuroimage 145, 24–43. https://doi.org/10.1016/j.neuroimage.2016.10.009.

Giovannoni, G., Tomic, D., Bright, J.R., Havrdová, E., 2017. No evident disease activity": the use of combined assessments in the management of patients with multiple sclerosis. Mult. Scler. J. 23, 1179–1187. https://doi.org/10.1177/1352458517703193.

Gros, C., De Leener, B., Badji, A., Maranzano, J., Eden, D., Dupont, S.M., Talbott, J., Zhuoquiong, R., Liu, Y., Granberg, T., Ouellette, R., Tachibana, Y., Hori, M., Kamiya, K., Chougar, L., Stawiarz, L., Hillert, J., Bannier, E., Kerbrat, A., Edan, G., Labauge, P., Callot, V., Pelletier, J., Audoin, B., Rasoanandrianina, H., Brisset, J.C., Valsasina, P., Rocca, M.A., Filippi, M., Bakshi, R., Tauhid, S., Prados, F., Yiannakas, M., Kearney, H., Ciccarelli, O., Smith, S., Treaba, C.A., Mainero, C., Lefeuvre, J., Reich, D.S., Nair, G., Auclair, V., McLaren, D.G., Martin, A.R., Fehlings, M.G., Vahdat, S., Khatibi, A., Doyon, J., Shepherd, T., Charlson, E., Narayanan, S., Cohen-Adad, J., 2019. Automatic segmentation of the spinal cord and intramedullary multiple sclerosis lesions with convolutional neural networks. Neuroimage 184, 901–915. https://doi.org/10.1016/j.neuroimage.2018.09.081.

Kearney, H., Miller, D.H., Ciccarelli, O., 2015. Spinal cord MRI in multiple sclerosis–diagnostic, prognostic and clinical value. Nat. Rev. Neurol. 11, 327–338. https://doi.org/10.1038/nrneurol.2015.80.

Lersy, F., Noblet, V., Willaume, T., Collongues, N., Kremer, L., Fleury, M., de Seze, J., Kremer, S., 2021. Identification and measurement of cervical spinal cord atrophy in neuromyelitis optica spectrum disorders (NMOSD) and correlation with clinical characteristics and cervical spinal cord MRI data. Rev. Neurol. 177, 85–92. https://doi.org/10.1016/j.neurol.2020.05.007 (Paris).

Lorenzi, R.M., Palesi, F., Castellazzi, G., Vitali, P., Anzalone, N., Bernini, S., Cotta Ramusino, M., Sinforiani, E., Micieli, G., Costa, A., D'Angelo, E., Gandini Wheeler-Kingshott, C.A.M., 2020. Unsuspected involvement of spinal cord in alzheimer disease. Front. Cell Neurosci. 14, 1–10. https://doi.org/10.3389/fncel.2020.00006.

Losseff, N.A., Webb, S.L., O'Riordan, J.I., Page, R., Wang, L., Barker, G.J., Tofts, P.S., McDonald, W.I., Miller, D.H., Thompson, A.J., 1996. Spinal cord atrophy and disability in multiple sclerosis. Brain 119, 701–708. https://doi.org/10.1093/brain/119.3.701.

Lukas, C., Bellenberg, B., Prados, F., Valsasina, P., Parmar, K., Brouwer, I., Pareto, D., Rovira, À., Sastre-Garriga, J., Gandini Wheeler-Kingshott, C.A.M., Kappos, L., Rocca, M.A., Filippi, M., Yiannakas, M., Barkhof, F., Vrenken, H., 2021. Quantification of cervical cord cross-sectional area: which acquisition, vertebra level, and analysis software? A multicenter repeatability study on a traveling healthy volunteer. Front. Neurol. 12, 88–89. https://doi.org/10.3389/fneur.2021.693333.

Lukas, C., Knol, D.L., Sombekke, M.H., Bellenberg, B., Hahn, H.K., Popescu, V., Weier, K., Radue, E.W., Gass, A., Kappos, L., Naegelin, Y., Uitdehaag, B.M.J., Geurts, J.J.G., Barkhof, F., Vrenken, H., 2015. Cervical spinal cord volume loss is related to clinical disability progression in multiple sclerosis. J. Neurol. Neurosurg. Psychiatry 86, 410–418. https://doi.org/10.1136/jnnp-2014-308021.

Mariano, R., Messina, S., Roca-Fernandez, A., Leite, M.I., Kong, Y., Palace, J.A., 2021. Quantitative spinal cord MRI in MOG-antibody disease, neuromyelitis optica and multiple sclerosis. Brain 144, 198–212. https://doi.org/10.1093/brain/awaa347.

Moccia, M., de Stefano, N., Barkhof, F., 2017. Imaging outcome measures for progressive multiple sclerosis trials. Mult. Scler. J. 23, 1614–1626. https://doi.org/10.1177/1352458517729456.

Moccia, M., Prados, F., Filippi, M., Rocca, M.A., Valsasina, P., Brownlee, W.J., Zecca, C., Gallo, A., Rovira, A., Gass, A., Palace, J., Lukas, C., Vrenken, H., Ourselin, S., Gandini Wheeler-Kingshott, C.A.M., Ciccarelli, O., Barkhof, F., 2019. Longitudinal spinal cord atrophy in multiple sclerosis using the generalized boundary shift integral. Ann. Neurol. 86, 704–713. https://doi.org/10.1002/ana.25571.

Moccia, M., Valsecchi, N., Ciccarelli, O., Van Schijndel, R., Barkhof, F., Prados, F., 2020. Spinal cord atrophy in a primary progressive multiple sclerosis trial: improved sample size using GBSI. Neuroimage Clin. 28, 102418 https://doi.org/10.1016/j.nicl.2020.102418.

Modat, M., Cash, D.M., Daga, P., Winston, G.P., Duncan, J.S., Ourselin, S., 2014. Global image registration using a symmetric block-matching approach. J. Med. Imaging 1, 024003. https://doi.org/10.1117/1.JMI.1.2.024003.

Nakamura, K., Eskildsen, S.F., Narayanan, S., Arnold, D.L., Collins, D.L., 2018. Improving the SIENA performance using BEaST brain extraction. PLoS ONE 13, e0196945. https://doi.org/10.1371/journal.pone.0196945.

Prados, F., Barkhof, F., 2018. Spinal cord atrophy rates. Neurology 91, 157–158. https://doi.org/10.1212/WNL.0000000000005873.

Prados, F., Cardoso, M.J., Leung, K.K., Cash, D.M., Modat, M., Fox, N.C., Wheeler-Kingshott, C.A.M., Ourselin, S., 2015. Measuring brain atrophy with a generalized formulation of the boundary shift integral. Neurobiol. Aging 36, S81–S90. https://doi.org/10.1016/j.neurobiolaging.2014.04.035.

Prados, F., Cardoso, M.J., Yiannakas, M.C., Hoy, L.R., Tebaldi, E., Kearney, H., Liechti, M.D., Miller, D.H., Ciccarelli, O., Wheeler-Kingshott, C.A.M.G., Ourselin, S., 2016. Fully automated grey and white matter spinal cord segmentation. Sci. Rep. 6, 36151. https://doi.org/10.1038/srep36151.

Prados, F., Moccia, M., Johnson, A., Yiannakas, M., Grussu, F., Cardoso, M.J., Ciccarelli, O., Ourselin, S., Barkhof, F., Wheeler-Kingshott, C., 2020. Generalised boundary shift integral for longitudinal assessment of spinal cord atrophy. Neuroimage 209, 116489. https://doi.org/10.1016/j.neuroimage.2019.116489.

Rovira, A., de Stefano, N., 2016. MRI monitoring of spinal cord changes in patients with multiple sclerosis. Curr. Opin. Neurol. 29, 445–452. https://doi.org/10.1097/WCO.0000000000000343.

Smith, S.M., Rao, A., De Stefano, N., Jenkinson, M., Schott, J.M., Matthews, P.M., Fox, N. C., 2007. Longitudinal and cross-sectional analysis of atrophy in Alzheimer's disease: cross-validation of BSI, SIENA and SIENAX. Neuroimage 36, 1200–1206. https://doi.org/10.1016/j.neuroimage.2007.04.035.

Smith, S.M., Zhang, Y., Jenkinson, M., Chen, J., Matthews, P.M., Federico, A., De Stefano, N., 2002. Accurate, robust, and automated longitudinal and cross-sectional brain change analysis. Neuroimage 17, 479–489. https://doi.org/10.1006/nimg.2002.1040.

Storelli, L., Pagani, E., Pantano, P., Piervincenzi, C., Tedeschi, G., Gallo, A., De Stefano, N., Battaglini, M., Rocca, M.A., Filippi, M., 2023. Methods for brain atrophy MR quantification in multiple sclerosis: application to the multicenter INNI dataset. J. Magn. Reson. Imaging. https://doi.org/10.1002/jmri.28616.

Stroman, P.W., Wheeler-Kingshott, C., Bacon, M., Schwab, J.M., Bosma, R., Brooks, J., Cadotte, D., Carlstedt, T., Ciccarelli, O., Cohen-Adad, J., Curt, A., Evangelou, N., Fehlings, M.G., Filippi, M., Kelley, B.J., Kollias, S., Mackay, A., Porro, C.A., Smith, S., Strittmatter, S.M., Summers, P., Tracey, I., 2014. The current state-of-the-art of spinal cord imaging: methods. Neuroimage 84, 1070–1081. https://doi.org/10.1016/j.neuroimage.2013.04.124.

Tur, C., Moccia, M., Barkhof, F., Chataway, J., Sastre-Garriga, J., Thompson, A.J., Ciccarelli, O., 2018. Assessing treatment outcomes in multiple sclerosis trials and in the clinical setting. Nat. Rev. Neurol. 14, 75–93. https://doi.org/10.1038/nrneurol.2017.171.

Tustison, N.J., Avants, B.B., Cook, P.A., Zheng, Yuanjie, Egan, A., Yushkevich, P.A., Gee, J.C., 2010. N4ITK: improved N3 bias correction. IEEE Trans. Med. Imaging 29, 1310–1320. https://doi.org/10.1109/TMI.2010.2046908.

Uher, T., Vaneckova, M., Sobisek, L., Tyblova, M., Seidl, Z., Krasensky, J., Ramasamy, D., Zivadinov, R., Havrdova, E., Kalincik, T., Horakova, D., 2017. Combining clinical and magnetic resonance imaging markers enhances prediction of 12-year disability in multiple sclerosis. Mult. Scler. J. 23, 51–61. https://doi.org/10.1177/1352458516642314.

Valsasina, P., Aboulwafa, M., Preziosa, P., Messina, R., Falini, A., Comi, G., Filippi, M., Rocca, M.A., 2018. Cervical cord T1-weighted hypointense lesions at MR imaging in multiple sclerosis: relationship to cord atrophy and disability. Radiology 288, 234–244. https://doi.org/10.1148/radiol.2018172311.

Valsasina, P., Horsfield, M.A., Meani, A., Gobbi, C., Gallo, A., Rocca, M.A., Filippi, M., 2022. Improved assessment of longitudinal spinal cord atrophy in multiple sclerosis using a registration-based approach: relevance for clinical studies. J. Magn. Reson. Imaging 55, 1559–1568. https://doi.org/10.1002/jmri.27937.

Wheeler-Kingshott, C.A., Stroman, P.W., Schwab, J.M., Bacon, M., Bosma, R., Brooks, J., Cadotte, D.W., Carlstedt, T., Ciccarelli, O., Cohen-Adad, J., Curt, A., Evangelou, N., Fehlings, M.G., Filippi, M., Kelley, B.J., Kollias, S., Mackay, A., Porro, C.A., Smith, S., Strittmatter, S.M., Summers, P., Thompson, A.J., Tracey, I., 2014. The current state-of-the-art of spinal cord imaging: applications. Neuroimage 84, 1082–1093. https://doi.org/10.1016/j.neuroimage.2013.07.014.

Yiannakas, M.C., Mustafa, A.M., De Leener, B., Kearney, H., Tur, C., Altmann, D.R., De Angelis, F., Plantone, D., Ciccarelli, O., Miller, D.H., Cohen-Adad, J., Gandini Wheeler-Kingshott, C.A.M., 2016. Fully automated segmentation of the cervical cord from T1-weighted MRI using PropSeg : application to multiple sclerosis. Neuroimage Clin. 10, 71–77. https://doi.org/10.1016/j.nicl.2015.11.001.

Ziegler, G., Grabher, P., Thompson, A., Altmann, D., Hupp, M., Ashburner, J., Friston, K., Weiskopf, N., Curt, A., Freund, P., 2018. Progressive neurodegeneration following spinal cord injury. Neurology 90, e1257–e1266. https://doi.org/10.1212/WNL.0000000000005258.